Monte Carlo simulation of diffusion in a $B2$-ordered model alloy

R. Weinkamer, P. Fratzl, B. Sepiol, and G. Vogl
Institut für Materialphysik der Universität Wien, Boltzmanngasse 5, A-1090 Wien, Austria
(Received 21 January 1998)

The diffusion process in a A-B binary alloy with $B2$ order is studied by atomistic Monte Carlo simulations using a vacancy mechanism. The chosen ordering energies were taken from neutron scattering experiments and ensure a phase diagram close to that of the real Fe-Al system. The dynamics was introduced by one single vacancy jumping to nearest-neighbor sites. Employing different jump-energy evaluations for the exchange vacancy and atom, we determined diffusion constants as a function of temperature and investigated the mobility of antiphase boundaries. While the different jump-energy evaluations yielded a similar behavior of the diffusion constant above T_c, we found a more complex influence of the evaluation on the diffusion constant below T_c. Finally, the autocorrelation function of the atoms was calculated and compared with measurements on $Fe_{50}Al_{50}$ done by quasielastic Mössbauer spectroscopy. A similarity between the simulated and the experimentally obtained autocorrelation function is observed despite the simplicity of the jump model used. [S0163-1829(98)05330-2]

I. INTRODUCTION

In many crystalline materials the elementary process of diffusion corresponds to the exchange between a vacancy and a neighboring atom. While this is well understood, e.g., for simple metals,[1] the diffusion process in $B2$ ordered intermetallic alloys is still not well understood. The main difficulty is that an exchange of the vacancy with a nearest-neighbor (NN) atom is associated with a local disturbance of the A-B ordering. In well-ordered alloys, e.g., at low temperatures, this implies an additional energetic barrier against diffusion. A number of possible jump mechanisms which might overcome this barrier without altering the long-range order have been proposed in the past. Typical examples are the classical six-jump cycle,[2] the antistructure bridge mechanism,[3] the triple-defect mechanism,[4] and antisite-assisted six-jump cycles.[5] As an alternative solution, elementary diffusion jumps to second and third nearest neighbors, i.e., within their own sublattice, have been suggested.

While tracer diffusion experiments allow only an indirect conclusion about the elementary diffusion jumps,[6,7] direct evidence could be gained by quasielastic Mössbauer spectroscopy (QMS),[8] quasielastic neutron scattering (QNS),[9] and recently nuclear forward scattering of synchrotron radiation (NFS).[10] These experimental techniques typically measure the autocorrelation function (or its Fourier transform) of a tagged atom in the alloy, with a time resolution corresponding to the life time τ_0 of the Mössbauer level for QMS and NFS (about 10^{-7} s) or the interaction time with the neutron for QNS (about 10^{-9} s).

The autocorrelation function gives information on the position of the tagged atom, initially located at the origin, after the time t. Recently, it has been deduced from QMS for the case of $B2$ FeAl that the Fe atoms effectively jump between sites on their own sublattice. These jumps are mostly to the third and, partly, to the second neighbor,[11,12] at least at 1065 °C. However, the QMS experiments provided evidence that they are a combination of two nearest-neighbor jumps.

A considerable effort is currently also undertaken by *ab initio* calculations and computer simulations using ''molecular statics'' and the embedded atom method,[13] as well as Monte Carlo (MC) simulations of simple models[5,14–18] to reach a better understanding of these phenomena. The *ab initio* calculations seem to indicate that vacancies practically cannot exist on the Al sublattice in $Fe_{50}Al_{50}$,[19] so that a direct jump of iron atoms to second neighbor positions (again located on the Fe sublattice) is proposed for the elementary diffusion jump.[20] MC simulations with a single vacancy, on the other hand, indicate that a simple nearest-neighbor exchange mechanism can explain a number of observations and even predicts a wealth of possible cyclic jumps occurring at low temperature,[5] among which is the well-known six-jump cycle.

Despite these efforts, a consistent picture for the elementary jump in $B2$ alloys has not yet emerged. In order to add some more pieces to this puzzle, we have undertaken a MC simulation of the diffusion process in a $B2$ model alloy focusing on the calculation of autocorrelation functions for comparison with QMS and NFS.

We chose to study the simplest possible Ising model with pair-interaction parameters as determined by diffuse neutron scattering for FeAl, the dynamics being provided by a single vacancy moving by nearest-neighbor jumps. To keep the number of parameters as small as possible, we take interaction parameters that guarantee equal probability for the vacancy to stay on either sublattice. We are aware that this assumption is not realistic. While the introduction of the vacancy does certainly not change the equilibrium properties of the Ising model significantly, the choice of the actual evaluation of the jump-energy may be expected to influence the dynamics, i.e., the diffusion process. To take this problem into account, we compare different evaluations and estimate the diffusion both at thermodynamic equilibrium and in the approach to equilibrium by monitoring the movement of antiphase boundaries (APB's). We then calculate diffusion constants as well as autocorrelation functions and compare them to available experimental data.

II. DESCRIPTION OF THE SIMULATION

A. The model

The Monte Carlo simulations have been performed on a rigid bcc lattice, using periodic boundary conditions to reduce finite-size effects. The typical lattice consisted of $N=32\times32\times64=65536$ sites, which were occupied by an equal number of atoms of type A (N_A) and B (N_B). The lattice was allowed to have one empty site representing a vacancy ($N_V=1$), substituting always a B atom ($N=N_A+N_B+1$, $N_B+1=N_A$). In a first approximation, only pair interactions $\varepsilon_{XY}^{(k)}$ were included into the Hamiltonian of this system, where X,Y equals A, B, or V. We took into consideration interactions up to the third nearest neighbors, i.e., $k=1,2$, or 3. In this so-called ABV model[21,22] the Hamiltonian can be written as

$$\mathcal{H}=\mathcal{H}_0+\sum_{k=1}^{3}\sum_{\langle i,j\rangle}^{k\text{th}}[K^{(k)}\sigma_i^2\sigma_j^2+J^{(k)}\sigma_i\sigma_j+U^{(k)}(\sigma_i^2\sigma_j+\sigma_i\sigma_j^2)], \tag{1}$$

where

$$K^{(k)}=\tfrac{1}{4}(\varepsilon_{AA}^{(k)}+\varepsilon_{BB}^{(k)}+2\varepsilon_{AB}^{(k)})+\varepsilon_{VV}^{(k)}-\varepsilon_{AV}^{(k)}-\varepsilon_{BV}^{(k)},$$

$$J^{(k)}=\tfrac{1}{4}(\varepsilon_{AA}^{(k)}+\varepsilon_{BB}^{(k)}-2\varepsilon_{AB}^{(k)}),$$

$$U^{(k)}=\tfrac{1}{4}(\varepsilon_{AA}^{(k)}-\varepsilon_{BB}^{(k)})-\frac{1}{2}(\varepsilon_{AV}^{(k)}-\varepsilon_{BV}^{(k)}).$$

The notation $\Sigma_{\langle i,j\rangle}^{k\text{th}}$ means summation over all kth nearest-neighbor pairs. The spin variable σ_i takes the values 1, -1, or 0, if there is an A atom, B atom, or vacancy at site i, respectively. The term $\mathcal{H}_0$, and—in our case of one single vacancy—also the first summand, are independent of the microscopic configuration of the atoms.

An alternative way of writing the interaction Hamiltonian is

$$\mathcal{H}=\mathcal{H}_0'-\sum_{k=1}^{3}[2J^{(k)}n_{AB}^{(k)}+U^{(k)}(n_{AV}^{(k)}-n_{BV}^{(k)})], \tag{2}$$

where $n_{XY}^{(k)}$ denotes the number of XY pairs of kth neighbors. This equation clearly shows that the constants $J^{(k)}$ essentially determine the ordering between A and B atoms, while the constants $U^{(k)}$ are responsible for the behavior of the vacancy. In particular, if $U^{(k)}>0$ (respectively, $U^{(k)}<0$) the vacancy prefers A atoms (respectively, B atoms) in its kth neighbor shell. For $U^{(k)}=0$, which is chosen here, there is no preference.

We have used the ordering energies $J^{(k)}$ adapted by Schmid and Binder[23] from diffuse neutron scattering experiments on Fe-Al.[24] With the appropriate temperature rescaling, we took $J^{(1)}=1$, defining the unit of energy, $J^{(2)}=0.167$ and $J^{(3)}=-0.208$. This model exhibits an order-disorder transition from the disordered $A2$ to the ordered $B2$ phase at $T_c=7.9J^{(1)}/k_B$.[23] Because of the low melting temperature of $Fe_{50}Al_{50}$ (1310 °C), this phase transition cannot be observed in the real alloy. The phase diagram of the A-B model is not expected to be changed by the introduction of a single vacancy.

All the dynamics was introduced by the movement of the single vacancy. In contrast to previous simulations,[14,25] only jumps to one of the eight nearest-neighbor positions were allowed. The problem of vacancy trapping in ordered regions did not emerge because of the rather large coordination number of the bcc lattice[26] ($Z_1=8$) on the one hand, and the moderate and high temperatures employed in our simulations on the other hand. The temperature T ranged from $0.46T_c$ up to infinity, excluding temperatures too close to the critical temperature.

The degree of order in the system was observed by order parameters in the usual way. The long-range order (LRO) parameter was defined as independent sum over both sublattices (α,β) with different sign ($\mathrm{LRO}=1/N(|\Sigma_\alpha\sigma_i-\Sigma_\beta\sigma_i|)$, while the ith short-range order parameter was set equal to the probability of finding a ith nearest-neighbor AB pair. All the simulations were repeated 25 or 50 times to improve their statistical reliability.

B. Jump-energy evaluations and algorithms

We used two different jump-energy evaluations for the vacancy and atom exchange to investigate the influence of the evaluation on the simulation results. The two possibilities for evaluating the energy change ΔE associated with the jump of the vacancy were (i) to take the difference between the energy of the final and the initial state or (ii) to introduce an energy barrier separating these two states. In (ii), the energy change ΔE was the saddle point energy minus the energy of the initial state and, therefore, was independent of the energy level reached after the jump. The height of the energy barrier was assumed to be higher than the energy of all possible configurations around the vacancy, i.e., $\Delta E>0$ in any case. In the following, the two different jump-energy evaluations are shortly designated as evaluation without barrier (i) and evaluation with barrier (ii). For both evaluations we compared (a) the standard Metropolis algorithm[27] with (b) a residence time algorithm (RTA).[28–30]

(a) Following the standard Metropolis algorithm the exchange probability of the vacancy with a randomly chosen NN atom i is given by

$$P_i=\min[1,\exp(-\Delta E/kT)]. \tag{3}$$

Hence, the probability of a vacancy-exchange with the NN atom i at exactly the τth trial, i.e., after $\tau-1$ unsuccessful trials, is

$$p_i^M(\tau)=(1-q)^{\tau-1}q\frac{P_i}{Z_1}, \tag{4}$$

with $q=(1/Z_1)\Sigma_{j=1}^{Z_1}P_j$. The time unit is usually defined as one Monte Carlo step (MCS), i.e., one attempted interchange per site.

(b) In contrast to the standard algorithm, the use of a residence time algorithm ensures that the vacancy performs a jump at each attempt. Here the exchange probabilities P_j are evaluated for each NN atom using the Metropolis rule (3).

Two random numbers between 0 and 1 are generated. The first R_1 serves for the determination of the exchanging atom i according to the inequality

$$\sum_{j=1}^{i-1} P_j/P \leqslant R_1 < \sum_{j=1}^{i} P_j/P, \tag{5}$$

where $P=qZ_1$ and the second R_2 yields the incrementation τ of the total time by

$$\tau = \frac{-\ln(R_2)}{q}. \tag{6}$$

For the conversion into MCS, τ has to be divided by N, the number of sites. Here τ denotes a continuous time and the probability of an atom and vacancy exchange i at τ is

$$p_i^R(\tau) = \exp(-q\tau) q \frac{P_i}{Z_1}. \tag{7}$$

The mean residence time $\overline{\tau}$ is equal for the standard Metropolis algorithm

$$\overline{\tau} = \sum_{\tau=1}^{\infty} \tau (1-q)^{\tau-1} q = \frac{1}{q}, \tag{8}$$

and for the residence time algorithm

$$\overline{\tau} = \int_0^{\infty} \tau \exp(-q\tau) q d\tau = \frac{1}{q}. \tag{9}$$

III. CALCULATION

A. Diffusion constants at thermal equilibrium

The conventional way of determining the tracer (respectively, vacancy) diffusion constant by means of computer simulations is to observe the mean-squared displacements of the tracer atoms (respectively, vacancy), for bcc lattices, see e.g., Ref. 31. For each given temperature, a run was not started until the lattice reached thermal equilibrium. This was controlled by comparing two runs starting from a perfectly ordered lattice, on the one hand, and from a random distribution of atoms, on the other. When both reached the same long-range order parameter, we considered to have attained equilibrium and started the determination of the diffusivities. The vacancy diffusion constant was calculated using[32]

$$D_V = \lim_{t\to\infty} \left(\frac{1}{6} \frac{\partial}{\partial t} R_V^2(t) \right), \tag{10}$$

where $R_V^2(t)$ denotes the mean-squared total displacement of the vacancy after a time t. Since all A atoms (B atoms) may individually be viewed as tracers, the tracer diffusion constant D_A (D_B) was calculated in the same way from

$$D_A = \lim_{t\to\infty} \left[\frac{1}{6N_A} \frac{\partial}{\partial t} \left(\sum_{A \text{ atoms}} R_A^2(t) \right) \right]. \tag{11}$$

In order to obtain adequate statistics the data were averaged over at least 50 independent simulation runs each going on for t up to 1000 MCS. The number of runs was increased at low temperatures because in this case the atoms performed only a small number of jumps per run. Since there was no asymmetry between A and B atoms ($U^{(k)}=0$), the values for D_A and D_B were equal and could be averaged additionally. Because only one vacancy was included in the system, it was also necessary to perform longer runs in order to reduce the large error bars for $R_V^2(t)$ in the determination of D_V.

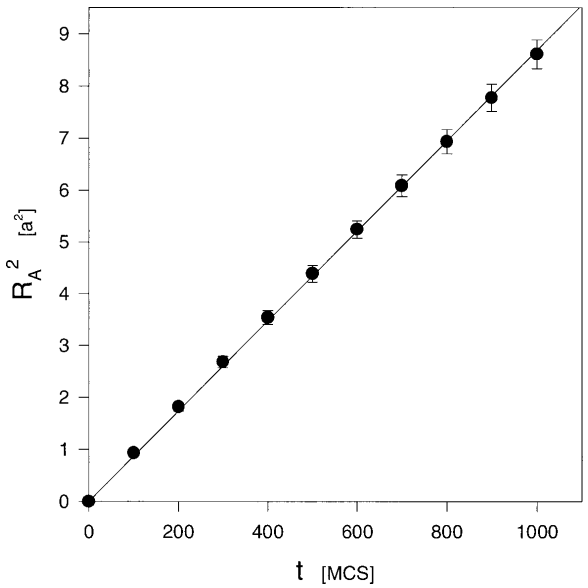

FIG. 1. The mean-squared displacement (relative to the lattice constant a) with standard deviation of the tracer atoms as a function of time; $T/T_c=0.65$, standard Metropolis algorithm without energy barrier. The diffusion constant is given by the slope times 1/6 for cubic lattices.

Figure 1 shows a typical plot of the mean-squared displacement of the tracer atoms versus time. The slope of the straight line, determined by a least squares fit, was used to calculate the diffusion constant.

B. Motion of antiphase boundaries

We also examined the motion of antiphase boundaries (APB's) at late stages of an ordering process. The starting point was the completely disordered state ($T=\infty$). After a quench well below the order-disorder transition (T_c), long-range order developed by nucleation and growth of ordered domains. In later stages the system consisted of a network of domain walls separating ordered regions (Fig. 2). In this so-called coarsening regime, the energy excess of the system was typically contained in the APB's. In good approximation, the deviation of the first short-range order (SRO) parameter from its equilibrium value can be taken proportional to the surface S of the APB's[33] ($\mathrm{SRO}_\infty - \mathrm{SRO} \propto S$). Since the volume of the ordered domains is approximately constant and roughly equal to the system size in this regime, S is correlated elementary with the mean domain size R by $S \propto 1/R$.

For a binary alloy undergoing an order-disorder transition, that is with nonconserved order parameter, an algebraic growth law $R(t) \propto (Mt)^x$ with $x=\frac{1}{2}$ has been proposed[34] (Allen-Cahn law), where M denotes the mobility of APB's. The power law $R(t) \propto t^x$ had been confirmed by MC simulations,[33] although the exponent was sometimes

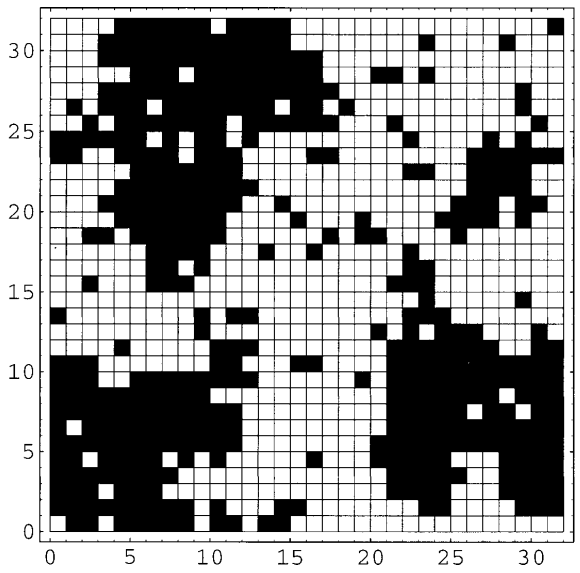

FIG. 2. Snapshot picture of the system [(100) plane] at the beginning of the coarsening regime. The image was prepared by overlaying a mask of $B2$ order. Therefore domains are distinguished by color.

larger than $\frac{1}{2}$ and could depend on temperature and dimensionality.[14] Summarizing, we expect to find the relation

$$\mathrm{SRO}-\mathrm{SRO}_{\infty}=K(Mt)^{-1/2}, \tag{12}$$

where K is a prefactor.

Figure 3 shows the short-range order parameter difference $\mathrm{SRO}-\mathrm{SRO}_{\infty}$ as a function of time$^{-1/2}$. A linear regime is observed over a long period of time, which is interpreted as the coarsening regime marked by open symbols. Naturally, the fitted straight line has to pass through zero in the limit $t\rightarrow\infty$. The same behavior is observed for both algorithms. Deviations from this behavior occurred at short and at very

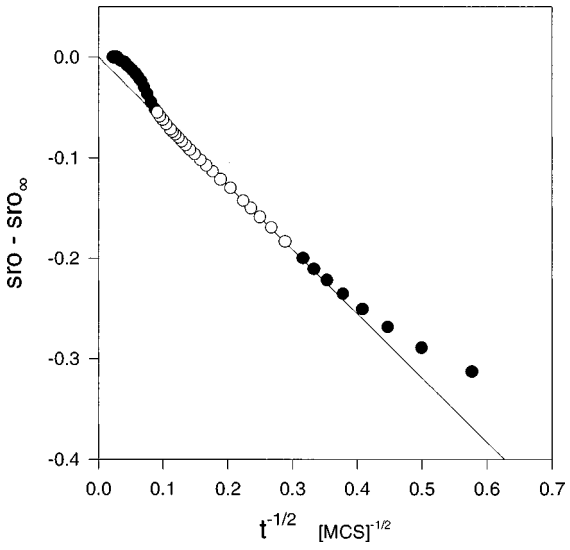

FIG. 3. The deviation of the first short-range order parameter from its equilibrium value plotted against $t^{-1/2}$. Open symbols mark the coarsening regime, where a linear correlation holds; $T/T_c=0.65$, standard Metropolis algorithm without energy barrier.

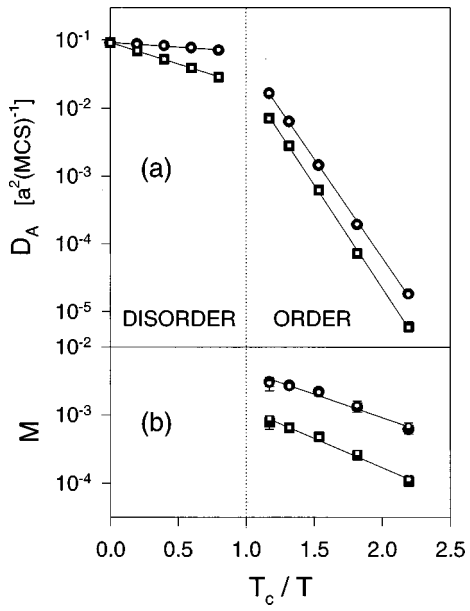

FIG. 4. Arrhenius plots of the common logarithm of the atom diffusivity versus inverse temperature calculated by observing (a) the mean-squared displacement of the atoms, (b) the movement of antiphase boundaries calculated using an jump-energy evaluation with barrier (circle) and without barrier (squares). Filled symbols correspond to a standard Metropolis algorithm, small open symbols to a residence time algortihm. Since the open, small, and filled large symbols superimpose almost perfectly, they look similar to one open symbol. Error bars are partly too small to be seen.

long times. At short times, there is a deviation from linearity before the beginning of the coarsening regime. A deviation can also be seen at very long times, when the mean domain size becomes comparable to the size of the whole system. Runs with smaller and larger lattices ($L=16$ and 64, $N=2L^3$) proved that this deviation was due to finite-size effects.

Since all points not belonging to the coarsening regime lie above the fitted line, we computed the mobility M from the minimum value of $t^{1/2}(\mathrm{SRO}-\mathrm{SRO}_{\infty})$. Averaging over 25 different runs, we excluded the cases that lead to final ''slab'' configurations, which were characterized by a very low value of the long-range order parameter, and corresponded to two competing domains separated by a flat interface.

IV. RESULTS AND DISCUSSION

A. Temperature dependence of diffusion constants

The atomic diffusion constant at equilibrium D_A and the mobility of APB's M were determined at temperatures below and above T_c and for all different updating jump-energy evaluations and algorithms (Fig. 4). As expected, there was no difference in the results obtained with the residence time or the standard Metropolis algorithm, neither for D_A nor for M. However, the use of an evaluation with barrier (ii) yielded smaller values for the diffusion constant at equilibrium than the evaluation (i), except in the limit of infinite temperature [Fig. 4(a)]. The values for D_A could be fitted by two straight lines as a function of $1/T$ for temperatures above and below T_c. The Arrhenius plot shows a change in slope

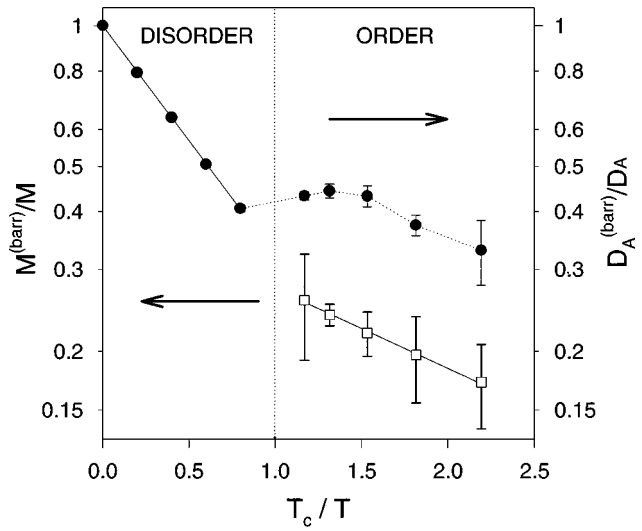

FIG. 5. Arrhenius plot of the ratio between D_A (circles) and M (squares) obtained by a jump-energy evaluation with and without barrier. Error bars denote standard deviations.

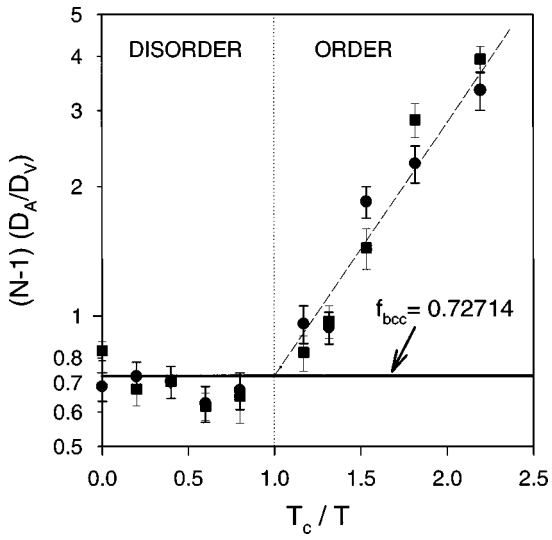

FIG. 6. Semilogarithmic graph of the ratio between the atom diffusivity and the vacancy diffusivity. Different symbols denote different evaluations of the jump energy. Error bars correspond to the standard deviation of the mean. The solid line marks the correlation factor of a bcc lattice.

at T_c, and the migration energy E_A^m is lower in the disordered phase ($1.0J^{(1)}$) than in the ordered phase ($23.0J^{(1)}$). This small value for E_A^m in the disordered phase is reasonable since there is no significant change in the environment of the vacancy before and after the jump, i.e., $\Delta E \approx 0$. For an algorithm with energy barrier the change by passing T_c is from $24.1J^{(1)}$ to $5.0J^{(1)}$. This large deviation from zero is due to the fact that the energy of a random environment around the vacancy is well below the defined energy barrier. As mentioned above, the height of the energy barrier is defined by the configuration around the vacancy with highest energy, which is a kind of wrong-ordered state.

In the limit $T \to \infty$, D_A is the same for all algorithms and can be calculated as follows. For cubic lattices the tracer diffusion coefficient is given by[35]

$$D_A = \frac{\Gamma r^2 f}{6}, \tag{13}$$

where Γ is the jump frequency ($\Gamma = 1$ [MCS^{-1}], because every jump trial is successful at $T = \infty$), r the NN distance ($r = a\sqrt{3}/2$), and f the correlation factor of bcc ($f_{\mathrm{bcc}} = 0.72714$),[35] and therefore $D_A^{T=\infty} = 0.09089$ [a^2MCS^{-1}] in perfect agreement with the simulated value.

Figure 4(b) shows the temperature dependence of the mobility M of APB's on the same scale. The temperature range is restricted to temperatures below T_c simply because only there do APB's exist. Again the data can be fitted by two straight lines, but in comparison with the case studied above, the slope is smaller. The activation energies were determined to $5.5J^{(1)}$ without barrier and $6.8J^{(1)}$ with barrier. The rather small energies can be understood in comparison with MC simulations that indicated that the vacancy path is mainly restricted to disordered regions.[22] As a consequence the vacancy is bound to the APB's and does not stray into the ordered domains.

Figure 5 shows the ratio of the results using the jump-energy evaluations with and without barrier for the APB mobility M as well as for the diffusion constant D_A. For D_A this ratio has an Arrhenius-type behavior for $T > T_c$ with a slope of $= 3.9J^{(1)}$. Therefore, employing an evaluation with barrier simply results in an additional activation energy. The same assertion holds for the mobility of APB's, although the additional energy is smaller ($1.3J^{(1)}$). Below T_c, the behavior is more complicated in the case of D_A. The full symbols obviously cannot be fitted by a straight line revealing a non-Arrhenian behavior of the diffusion constants. Moreover, the open and full symbols in Fig. 5 do not superimpose, which means that the consideration of an activation barrier in the energy evaluation has changed the mobility of A atoms and of APB's in a different way.

B. Ratio of atom diffusion to vacancy diffusion

In Fig. 6 the ratio between the atom diffusivity (multiplied by the number of atoms $N-1$) and the vacancy diffusivity is plotted against the inverse temperature scale T_c/T. The data points scatter around two straight lines subdividing the diagram into two temperature ranges above and below the ordering energy. Above T_c, the ratio $f = (N-1)D_A/D_V$ equals the diffusion correlation coefficient of a bcc lattice ($f_{\mathrm{bcc}} = 0.72714$),[35] which means that the system behaves as a conventional bcc lattice. Below T_c, the ratio increases with decreasing temperature, f taking values larger than 1.

This effect may be explained by highly correlated vacancy sequences. Using improved residence algorithms Athènes *et al.*[5] showed that at sufficiently low temperatures ($T/T_c < 0.3$) six-jump cycles are the only contribution to atomic migration. For intermediate temperatures antisites are integrated into the six-jump cycles lowering the activation energy (anitsite-assisted six-jump cycle). This concept of antisite-assisted cycles can be extended, especially at higher temperatures when more antisites are present in the system and therefore can be involved into jump cycles. The outcome of these jump cycles is a low net migration of the vacancy without preventing the atom diffusion as observed in our

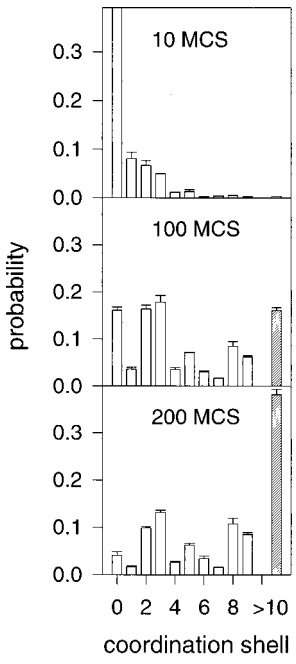

FIG. 7. Autocorrelation function of the A atoms after $t=10$, 100, and 200 MCS; $T/T_c=0.76$, standard Metropolis algorithm without energy barrier. The last, hatched bar represents the probability of finding an iron atom in the tenth or higher coordination shell.

simulation. At temperatures close to T_c and decreasing long-range order the vacancy is not restricted to such jump cycles anymore since a combined destruction and restoration of the lattice order take place. Above T_c the vacancy basically performs a random walk.

C. Autocorrelation function

Figure 7 shows the probability of finding an A atom, located at the origin at $t=0$, in the kth coordination shell after a time t. Since the simulation yielded the displacement vector for each atom as a function of time (Sec. III A), we obtained the autocorrelation function by counting the atoms with the same total displacement, i.e., atoms within the same coordination shell. The simulations were performed with the standard Metropolis algorithm without barrier at $0.76T_c$. The consideration of an energy barrier had no influence on the results within the small error bars, except a time dependence. At the given temperature it took almost four times longer to obtain the same probability distribution of the A atoms than with a jump-energy evaluation without barrier. By definition all the A atoms are located in the zeroth shell for $t=0$ MCS. After $t=10$ MCS, the predominant part of the A atoms did not move or jumped back to their starting point. The bar at position 0 still does not fit in the diagram (top of Fig. 7). The probability of finding an A atom typically decreases with the index of the coordination shell. The situation changed after $t=100$ MCS. Just under 20% of the atoms did effectively not move. The first neighbor shell is poorly occupied, whereas the second and third shell house most of the A atoms, namely, 20% each. Note that at this time also about 20% of the A atoms reached the tenth or higher coordination shell. The salient feature after 200 MCS, finally, is that the third neighbor shell exceeds the second one clearly. The first shell is almost deserted. More than 35% of the atoms jumped further than the ninth shell.

These results are quite interesting in comparison to measurements on the Fe-Al system done by QMS (Ref. 11) and NFS.[12] A reasonable fit of the experimental data was obtained under the assumption that iron atoms jump between sites on their own sublattice. There is a preference of jumps to a third nearest-neighbor site ([110] jumps) over jumps to a second nearest-neighbor site ([100] jumps) with a probability ratio W_{110}/W_{100} of 1.7. The authors concluded that the jump is, however, not a direct one, but rather a combination of two nearest-neighbor jumps leading to a short-time occupation of an antistructure site on the Al sublattice.

Ab initio calculations also increased the doubt that iron atoms jump directly on their own sublattice. While the calculations for the direct jump of an Fe atom to a (100) site resulted in a migration energy of 2.41 eV,[20] direct [110] jumps can be excluded because of the extremely high migration energy of 6.36 eV.[36]

For comparison with the autocorrelation function obtained by the MC simulations, we calculated the autocorrelation function with the jump probabilities taken from the QMS experiments. The preference of [110] jumps over [100] jumps is reflected in the approximately time-independent higher occupation of the third with respect to the second nearest-neighbor shell, again with a ratio of roughly 1.7.

Now, our MC simulations, which are based on the assumption that diffusion proceeds via vacancy jumps to NN sites exclusively, also give a higher probability that the atoms end up on a third nearest-neighbor site after a time larger than 70 MCS. This is surprising at first glance, since an atom, which has just jumped to a NN site, has an equal number of possibilities to jump either to a second or to a third neighbor, namely, 3. Taking into consideration the correlated movement of the vacancy, the situation gets even worse. Calculations performed about the six-jump cycle found that the probability ratio even should rather be in favor of (100) jumps.[37] This tendency is reversed, however, if all the atoms had a sufficient large number of interchanges with the vacancy. Then, there are many more indirect paths to a third neighbor site than there are to a second, the reason being simply that in the bcc lattice there are twice as many third neighbors than second neighbors (12:6).

This similarity of the simulated autocorrelation function with the main feature of the experimental autocorrelation function is remarkable. It may indicate the possibility to reproduce the experimental results with an even simpler jump model than proposed earlier.[11] We are currently working to improve the model and the simulations in order to allow a more direct and more quantitative comparison with QMS results.

ACKNOWLEDGMENTS

We thank I. Žižak for assistance with the computer simulations and for helpful discussions. This work was supported by grants from the Austrian FWF (Project No. S5601).

[1] J. Philibert, *Atom Movements* (Les Éditions de Physique, Les Ulis, 1991).
[2] E. W. Elcock and C. W. McCombie, Phys. Rev. **109**, 605 (1958).
[3] C. R. Kao and Y. A. Chang, Intermetallics **1**, 237 (1993).
[4] N. A. Stolwijk, M. van Gand, and H. Bakker, Philos. Mag. A **42**, 783 (1980).
[5] M. Athènes, P. Bellon, and G. Martin, Philos. Mag. A **76**, 565 (1997).
[6] For an overview see H. Mehrer, Mater. Trans., JIM **37**, 1259 (1996).
[7] For the FeAl system see M. Eggersmann, B. Sepiol, G. Vogl, and H. Mehrer, Defect Diffus. Forum **143-147**, 339 (1997).
[8] G. Vogl, in *Mössbauer Spectroscopy Applied to Magnetism and Materials Science*, edited by Gary J. Lang and Fernande Grandjean (Plenum, New York, 1996), Vol. 2, and references therein.
[9] M. Bée, *Quasielastic Neutron Scattering* (Adam Hilger, Bristol, 1988).
[10] B. Sepiol, A. Meyer, G. Vogl, R. Rüffer, A. I. Chumakov, and A. Q. R. Baron, Phys. Rev. Lett. **76**, 3220 (1996).
[11] G. Vogl and B. Sepiol, Acta Metall. Mater. **42**, 3175 (1994).
[12] B. Sepiol, C. Czihak, A. Meyer, G. Vogl, J. Metge, and R. Rüffer (unpublished).
[13] Y. Mishin and D. Farkas, Philos. Mag. A **75**, 187 (1997).
[14] C. Frontera, E. Vives, and A. Planes, Z. Phys. B **96**, 79 (1994).
[15] L. Anthony and B. Fultz, J. Mater. Res. **9**, 348 (1994).
[16] K. Yaldram, V. Pierron-Bohnes, M. C. Cadeville, and M. A. Khan, J. Mater. Res. **10**, 591 (1995).
[17] I. V. Belova, M. E. Ivory, and G. E. Murch, Philos. Mag. A **72**, 871 (1995).
[18] G. Yu, Phys. Status Solidi B **203**, 313 (1997).
[19] J. Mayer, C. Elsässer, and M. Fähnle, Phys. Status Solidi B **191**, 283 (1995).
[20] J. Mayer and M. Fähnle, Defect Diffus. Forum **143-147**, 285 (1997).
[21] K. Yaldram and K. Binder, J. Stat. Phys. **62**, 161 (1991).
[22] E. Vives and A. Planes, Int. J. Mod. Phys. C **4**, 701 (1993).
[23] F. Schmid and K. Binder, J. Phys.: Condens. Matter **4**, 3569 (1992).
[24] V. Pierron-Bohnes, S. Lefevbre, M. Bressiere, and A. Finel, Acta Metall. **38**, 2701 (1991).
[25] P. A. Flinn and G. M. McManus, Phys. Rev. **124**, 54 (1961).
[26] B. Fultz and L. Anthony, Philos. Mag. Lett. **59**, 237 (1989).
[27] N. Metropolis, A. W. Rosenbluth, M. N. Rosenbluth, A. H. Teller, and E. Teller, J. Chem. Phys. **21**, 1087 (1953).
[28] A. B. Bortz, M. H. Kalos, and J. L. Lebowitz, J. Comput. Phys. **17**, 10 (1975).
[29] Y. Limoge and J. L. Bocquet, Acta Metall. **36**, 1717 (1988).
[30] T. A. Abinandanan, F. Haider, and G. Martin, Key Eng. Mater. **103**, 87 (1995).
[31] H. Bakker, N. Stolwijk, L. P. Van der Meij, and T. Zuurendonk, Nucl. Metall., Metall. Soc. AIME (US) **20**, 96 (1976).
[32] L. Zhao, R. Najafabadi, and D. J. Srolovitz, Acta Mater. **44**, 2737 (1996).
[33] M. K. Phani, J. L. Lebowitz, M. H. Kalos, and O. Penrose, Phys. Rev. Lett. **45**, 366 (1980).
[34] S. M. Allen and J. W. Cahn, Acta Metall. **27**, 1085 (1979).
[35] See, e.g., G. E. Murch, in *Materials Science and Technology*, edited by R. W. Cahn, P. Haasen, and E. J. Kramer (VCH Verlagsgesellschaft, Weinheim, 1991), Vol. 5, Chap. 2.
[36] B. Meyer and M. Fähnle (private communication).
[37] M. Arita, M. Koiwa, and S. Ishioka, Acta Metall. **37**, 1363 (1989).